MNRAS 000, 1–9 (2022) Preprint 28 July 2022 Compiled using MNRAS LATEX style file v3.0

A Classification of Time-Variable Absorption of Gamma-Ray Bursts In Active Galactic Nuclei Accretion Disks

Michael Ray,[1]★
[1]Stony Brook University

Submitted as a thesis for the M.A. degree in physics at Stony Brook University on August 1, 2022.

ABSTRACT

Both long and short gamma-ray bursts are expected to occur in the dense environments of active galactic nuclei accretion disks. As these bursts emerge from the disks they live in, they photoionize the medium resulting in a time-dependent medium opacity that yields highly unusual transients that can be observed from outside the disk. In this paper, we simulate this radiation transfer in the case of long gamma-ray bursts to investigate the parameter space in which dense environments leave a significant and time-variable imprint on the bursts. Through our numerical investigation, we find that this interesting absorption occurs for $10^{56}(\frac{H}{1\text{ cm}})^{-3} \leq \frac{n_0}{1\text{ cm}^{-3}} \leq 10^{59}(\frac{H}{1\text{ cm}})^{-3}$, where n_0 is the initial number density of neutral Hydrogen in the plane of the accretion disk, and H is the scale height of the density profile of the disk under the assumption that the density falls off as a gaussian away from the plane of the disk. We then transform our findings in the (n_0, H) parameter space to findings in the (disk location, SMBH mass) parameter space, under the assumption of two different popular AGN accretion disk models.

Key words: radiative transfer – gamma-ray bursts – accretion, accretion disks

1 INTRODUCTION

Gamma-ray bursts (GRBs) are among the most energetic events in the Universe, capable of producing peak observed bolometric luminosities greater than 10^{53} erg s^{-1} (Gehrels et al. 2009). They come in two varieties, long and short, which are distinguished based on the time-scale in which they emit (Kouveliotou et al. 1993). Short GRBs are commonly taken to be those which emit for two seconds or less and are believed to result from compact object mergers (Fong & Berger 2013; Belczynski et al. 2006; Mochkovitch et al. 1993), while long GRBs are those which last longer than two seconds and are believed to result from the collapse of massive stars (Hjorth et al. 2003; Stanek et al. 2003). Because of their enormous energy output, both long and short GRBs can be seen from across the observable Universe, making them ideal sources to use to study distant galaxies. The early-time emission of GRBs (typically called the "prompt emission") tends to have complex time variability and is generally described by a simple broken power law with just three parameters (Band et al. 1993), while the late-time emission of GRBs (called the "afterglow emission") displays a simple, featureless power-law spectrum (Achterberg et al. 2001; Spitkovsky 2008).

Due to the simplicity of their afterglow spectra, GRBs are also ideal candidates to use to probe the medium in which they are emitted by observing the absorption lines imprinted on their spectra. While time-dependent absorption of GRB spectra in various media has been studied extensively (see e.g. Böttcher et al. 1999; Lazzati et al. 2001; Robinson et al. 2009; Campana et al. 2021), bursts in the environment of Active Galactic Nuclei (AGN) accretion disks is a relatively new area of research with few dedicated studies thus far (for studies that have already been performed, see e.g. Perna et al. 2021a; Yuan et al. 2021; Zhu et al. 2021b,a).

Active Galactic Nuclei (AGNs) are galactic centers with much higher than normal luminosity that is not characteristic of stellar emission. The emission from AGNs is believed to be driven by the accretion of a hot, magnetized plasma onto a central supermassive black hole (SMBH; Krawczynski & Treister 2013). While this accretion process is well understood, there is notable time variability observed in AGN spectra that has yet to be fully explained (Peterson 2001). Some have suggested that this variability is the result of stochastic temperature fluctuations in the accretion disk modelled by a damped random walk (Kelly et al. 2009; MacLeod et al. 2010; Ivezić & MacLeod 2014; Kozłowski 2016) while others have cast doubt on whether this is a viable model of AGN variability (Zu et al. 2013; Mushotzky et al. 2011; Kasliwal et al. 2015). An alternative and perhaps complementary explanation to the damped random walk model is that AGN variability is caused by GRBs emitted from within the AGN accretion disk. This explanation is made more plausible by the observation that AGN accretion disks are dense environments that carry stars which have the potential to emit long GRBs at the end of their lives, and compact objects such as neutron stars and stellar-mass black holes, which have the potential to emit short GRBs when they collide. While we constrain ourselves to GRBs in this paper, AGN disks are also expected to host various events capable of producing electromagnetic transients such as tidal disruption events (Yang et al. 2021), accretion-induced collapse of neutron stars (Perna et al. 2021b), core-collapse supernova (Grishin et al. 2021; Cantiello et al. 2021), and binary black hole mergers (Graham et al. 2020; Gröbner, M. et al. 2020).

In this paper, we perform a preliminary study of the effect that dense environments (such as AGN accretion disks) have on long GRB

★ E-mail: michael.ray.1@stonybrook.edu

(LGRB) spectra (we leave short GRBs to be investigated in a follow-up study). We perform a grid of simulations to solve for the conditions under which dense environments will have a meaningful and time-variable effect on LGRB spectra that are emitted from within the environment (the precise meaning of "meaningful and time-variable effect" is given in section 3). More specifically, since the early, high energy radiation from the GRB photoionizes the medium, it results in a time-dependent medium opacity during the early life of the transient. Since the medium opacity affects any spectra from the X-rays through the optical band, the combination of the intrinsic GRB spectrum with a variable opacity can produce unusual transients, which may be hard to recognize. To study and quantify this effect, we use a radiation transfer code presented in Perna & Lazzati (2002); this allows us to calculate the transformation that the dense environment induces on the GRB spectrum.

For our grid of simulations, we compute the radiation transfer for different central number densities of neutral atomic Hydrogen (n_0) and different scale heights, H (which effect the density profile of the medium), allowing us to derive the conditions on n_0 and H such that the surrounding medium will leave an interesting imprint on GRB spectra. After deriving these conditions on n_0 and H, we transform them into conditions on the physical parameters of AGN by choosing specific models of AGN accretion disks given by Thompson et al. (2005); Sirko & Goodman (2003). The physical parameters we map to are the location of the GRB in the AGN (distance from the SMBH) and the mass of the SMBH. In this way, we derive constraints on the physical parameters of the burst and AGN such that the environment strongly impacts the burst spectrum in a time-variable manner.

This study is organized as follows: in §2 we present the setup of the simulations including a description of how the radiation transfer code works, a description of the GRB luminosity functions used, as well as a description of the density and temperature profiles used. In §3 we present a detailed description of the simulations performed and the (n_0, H) parameter space that is covered. We then present the results of these simulations. In §4 we discuss the conclusions that can be drawn from the study and we also comment on future work to be done to extend and generalize the findings of this study.

2 SIMULATION SETUP

2.1 Choice of central densities and density profiles

The radiative transfer code used is flexible to any density and temperature profile desired. Here, our goal is to measure where, in (n_0, H) parameter space, the effect of absorption is significant. To find this area in the parameter-space, we perform a grid of simulations for all possible cominations of n_0 and H from the following lists:

n_0 [cm^{-3}] $\in \{10^4, 10^5, 10^6, 10^7, 10^8, 10^9, 10^{10}\}$,

H [cm] $\in \{10^{14}, 10^{15}, 10^{16}, 10^{17}, 10^{18}, 10^{19}, 10^{20}\}$.

We exclude any combinations of n_0 and H where the column density, $N_H = n_0 H$, is greater than 10^{24} cm^{-2}. This is because at column densities greater than 10^{24} cm^{-2}, the medium becomes optically thick to Thompson scattering (Wang et al. 2022), which is not included as an effect in the code we use for the simulations.

After picking a value for n_0, we can obtain the central mass density, ρ_0, by taking $\rho_0 = n_0 m_p$, where m_p is the mass of the proton. We then take the density of the medium along the z-axis (taking z to be the line-of-sight coordinate) as an (unnormalized) Gaussian with mean $z = 0$ and standard deviation H.

$$\rho(z) = \rho_0 \exp\left(\frac{-z^2}{2H^2}\right) . \quad (1)$$

One should take note, based on this discussion, that our results are not necessarily particular to AGN disks. In fact, this analysis will apply to GRBs that are emitted in any location where the density along the line-of-sight falls off as a Gaussian with mean $z = 0$. Accretion disks, and in particular AGN accretion disks, do happen to follow this density model and also happen to be an interesting area of research at this time, which justifies our focus on them.

2.2 GRB Luminosity Functions

We model the GRB luminosity as the sum of a prompt emission component and an afterglow component such that the total luminosity curve is given as:

$$L(t, \nu) = L_p(t, \nu) + L_{AG}(t, \nu) , \quad (2)$$

where $L_p(t, \nu)$ is the luminosity function for the prompt emission and $L_{AG}(t, \nu)$ is the luminosity function for the afterglow. For the prompt emission, the luminosity separates into a time-dependent component and a frequency-dependent component, that is:

$$L_p(t, \nu) = A_p T_p(t) F_p(\nu) \quad (3)$$

where A is a normalization constant. For the afterglow emission, we use a code that numerically computes afterglow emission in a given environment and we then fit analytical luminosity curves to the output of the computation.

2.2.1 *Prompt Emission*

We model the Long GRB (LGRB) prompt emission in a nearly identical way to Robinson et al. (2009). In their model, the functions $T_p(t)$ and $F_p(\nu)$ are each independently normalized such that $\int_0^\infty F_p(\nu) d\nu = 1$ and $\int_0^\infty T_p(t) dt = 1$. This ensures that the constant A_p contains all of the normalization for the prompt emission luminosity function. The time-dependent component of the prompt emission for the LGRB takes the form of a Gaussian with mean 10 seconds and full width half max 10 seconds (Robinson et al. 2009). Thus,

$$T_p(t) = A_{pt} \exp\left[\frac{-8ln(2)(t-10)^2}{200}\right] , \quad (4)$$

where t is measured in seconds. Normalizing such that $\int_0^\infty T_p(t) dt = 1$ gives $A_{pt} = 1.00935$ sec^{-1}.

The frequency-dependent component of the LGRB prompt emission takes after the spectrum given in Band et al. (1993) and is modeled by a broken power-law as:

$$F_p(E) = A_{pf} \left(\frac{E}{100 \text{ keV}}\right)^\alpha \exp\left(-\frac{E}{E_0}\right), (\alpha - \beta)E_0 \geq E \quad (5)$$

$$F_p(E) = A_{pf} \left[\frac{(\alpha-\beta)E_0}{100 \text{ keV}}\right]^{\alpha-\beta} \exp(\beta-\alpha) \left(\frac{E}{100 \text{ keV}}\right)^\beta , (\alpha - \beta)E_0 < E \quad (6)$$

where (α - β) E_0 is the knee of the power-law taken to be 300 keV

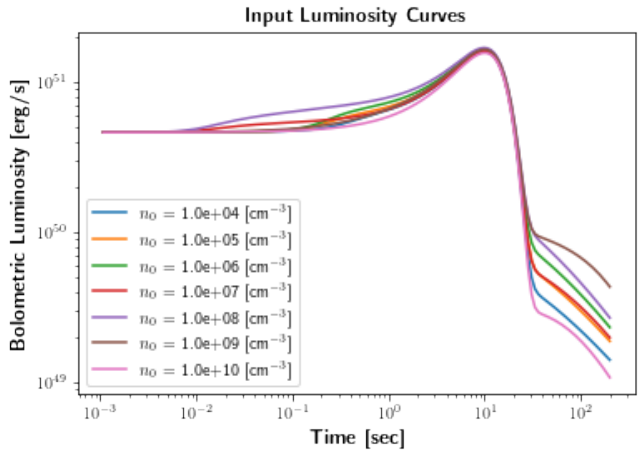

Figure 1. Input bolometric luminosity as a function of time for each of the afterglow models laid out in table 1. Each of the input lightcurves has the same prompt emission model, which is presented in section 2.2.1.

(i.e. this is the energy at which the luminosity function "turns over"), α is the slope of $F_p(E)$ for $E \leq E_0$ and β is the slope of $F_p(E)$ for $E > E_0$, and A_{pf} is a normalization constant. We use $\alpha = 0$ and $\beta = -2$ in our models. For these values of α and β it is easy to solve the equation $\int_0^\infty F(E)dE = 1$ for A_{pf}. Doing this leads to $A_{pf} = 2.935990 \times 10^{-3}$ keV^{-1}. Thus, we arrive at the prompt emission light curve given by:

$$L_p = A_p T_p(t) F_p(E) \tag{7}$$

where $T_p(t)$ and $F_p(E)$ are defined above. The constant A_p is the total energy output of the prompt emission, given by $A_p = \int_{t=0}^\infty \int_{\nu=0}^\infty L_p(t,\nu)d\nu dt$. Here we take $A_p = 10^{53}$ ergs.

2.2.2 *Afterglow Emission*

While GRB afterglows are still a current topic of active research (see e.g. Wang et al. (2022) or Golant & Sironi (2022)), it is currently understood that afterglows for both short and long GRBs are synchrotron radiation resulting from the collision of a relativistic shell with an external medium (Sari et al. 1998; Panaitescu & Kumar 2000). The relativistic shell here can be the result of, for instance, a supernova (for long GRBs) or the collision of two neutron stars (for short GRBs). The nature of the source of afterglow emission is such that the best way to compute afterglows is to simulate this shell/medium collision and compute the synchrotron radiation produced. To compute our afterglows, we used a code that has been used in various previous papers (Lazzati et al. 2018; Perna et al. 2022) and performs the afterglow computation numerically. We then fit a typical afterglow lightcurve to the numerically computed curves. The fit that we use for each of the curves assumes a broken power-law shape in both time and frequency and assumes standard parameters for the shell/medium collision (Sari et al. 1998; Panaitescu & Kumar 2000; Granot et al. 2002; Rossi et al. 2002). Since the shell/medium collision dynamics will depend on the density of the medium in the immediate vicinity of the burst, each afterglow model with a different value of n_0 will have different parameters. The value of the scale height does not affect the input GRB spectrum and thus does not enter into this calculation. The scale height will, however, affect the absorption of the input spectrum, and thus will affect the output spectrum observed. The luminosity curves for the afterglows of all input GRBs are shown in table 1. The total luminosity curves themselves are shown in figure 1 as a function of time.

2.3 Numerical Setup and Code Description

At the core of the simulations performed is a radiation transfer code which takes into account the time-dependent photo-ionization of both dust and metals in a medium subjected to an intense radiation field (Perna & Lazzati 2002). The code computes, on a 2-d space-time grid (one line-of-sight spatial coordinate and one time coordinate), the state of the radiation field, the abundance and ionization states of both molecular and atomic Hydrogen, and the abundance and ionization states of the 12 next most common astrophysical elements: He, C, N, O, Ne, Mg, Si, S, Ar, Ca, Fe, Ni (Perna & Lazzati 2002). In addition to storing the state of the medium and radiation field at each grid point, the code stores the output flux spectrum (that is, the flux emanating from the outermost bin along the z-axis, located at z_{max}) and the (frequency-dependent) optical depth, both as functions of time. In this way, the code produces for us a time-dependent optical depth spectrum and a time-dependent flux spectrum which fully describes the radiation that emerges from the AGN environment and flows freely to an observer. The radiative transfer is calculated in the energy range of 1 eV to 50 keV and throughout the calculations, energies are binned into 200 equally spaced bins.

When setting up the space-time grid, we take the start time, t_i, to be 10^{-3} seconds and the end time, t_f, to be 200 seconds with 1500 logarithmically spaced time steps. We take the minimum z-coordinate to be $z_{min} = 1.25 \times 10^{-3} H$ where H is the scale height of the AGN and the constant in front is chosen such that 0.1% of the total mass is contained within z_{min}. The maximum z-coordinate is chosen to be $z_{max} = 2.58H$ where the constant is chosen such that 99% of the total mass is contained within z_{max}. The interval $[z_{min}, z_{max}]$ is split into 100 logarithmically spaced steps.

We take the temperature to be 10^4 K in all simulations regardless of the values of n_0 and H. The constant temperature choice is motivated by the fact that the radiative transfer is much more sensitive to the density of the medium than the temperature of the medium. This phenomenon can be understood by noting that no matter what the temperature of the medium begins at, over a short period of time it will be heated by the GRB radiation to a value that depends largely on the GRB radiation itself, and for the most part not the initial temperature of the medium. Thus, the simulations should be relatively unchanged if we increase or decrease the initial temperature.

3 SIMULATION DESCRIPTION AND RESULTS

Our goal is to identify the area of the (n_0, H) parameter space in which we get significant absorption of our burst. What remains to be defined, however, is what we mean by "significant absorption". We propose the following three rules to determine whether "significant absorption" has occurred.

- $\tau_{0.1-10}(t_f) < 1$
- $\tau_{0.1-10}(0.1 \text{ sec}) > 0.7$
- $\tau_{0.1-10}(0.1 \text{ sec})/\tau_{.1-10}(t_f) > 2$

In these rules, $\tau_{0.1-10}(t)$ is defined as the average optical depth between energies 0.1 keV and 10 keV and t_f is the maximum time of the simulation, taken to be 200 seconds here. These rules ensure three things about the simulation:

- $\tau_{0.1-10}(t_f) < 1$ ensures that at the end of the simulation, we

Table 1. Afterglow models for every initial neutral Hydrogen density, n_0.

n_0 [cm^{-2}]	Long GRB Afterglow Model [erg/s/Hz]
10^4	$L(t,\nu) = 3\times10^{38}(\frac{10^{17}}{\nu})^{1.175}\left[5\times10^{5}(\frac{\nu}{10^{17}})^{-.65}t^{-3} + 5\times10^{14}(\frac{\nu}{10^{14}})^{-3.3}t^{-.85} + 10^{7}(\frac{\nu}{10^{17}})^{-.75} + 2\times10^{4}t^{1.1} + t^{2.1}\right]^{-1}$
10^5	$L(t,\nu) = 4.3\times10^{38}(\frac{10^{17}}{\nu})^{1.175}\left[10^{5}(\frac{\nu}{10^{17}})^{-.65}t^{-3} + 5\times10^{16}(\frac{\nu}{10^{14}})^{-3.3}t^{-.85} + 10^{7}(\frac{\nu}{10^{17}})^{-.75} + 2\times10^{4}t^{1.1} + (\frac{\nu}{10^{17}})^{-1}t^{2.1}\right]^{-1}$
10^6	$L(t,\nu) = 2\times10^{38}(\frac{10^{17}}{\nu})^{1.175}\left[3\times10^{4}(\frac{\nu}{10^{17}})^{-.65}t^{-3} + 3\times10^{17}(\frac{\nu}{10^{14}})^{-3.3}t^{-.85} + 3\times10^{6}(\frac{\nu}{10^{17}})^{-.75} + 7\times10^{3}t^{1.1} + t^{2.1} + 10^{9}(\frac{\nu}{10^{14}})^{-3.2}t^{1.5}\right]^{-1}$
10^7	$L(t,\nu) = 7.5\times10^{37}(\frac{10^{17}}{\nu})^{1.175}\left[10^{5}(\frac{\nu}{10^{17}})^{-3}t^{-3} + 3\times10^{8}(\frac{\nu}{10^{17}})^{-3.3}t^{-.85} + 2\times10^{6}(\frac{\nu}{10^{17}})^{-.75} + 2\times10^{3}t^{1.1} + t^{2.1} + 10^{11}(\frac{\nu}{10^{14}})^{-3.2}t^{1.5}\right]^{-1}$
10^8	$L(t,\nu) = 1.7\times10^{38}(\frac{10^{17}}{\nu})^{1.175}\left[10^{5}(\frac{\nu}{10^{17}})^{-3}t^{-3} + 3\times10^{9}(\frac{\nu}{10^{17}})^{-3.3}t^{-.85} + 8\times10^{7}(\frac{\nu}{10^{17}})^{-1.75} + 2\times10^{3}t^{1.1} + t^{2.1} + 10^{13}(\frac{\nu}{10^{14}})^{-3.5}t^{1.5}\right]^{-1}$
10^9	$L(t,\nu) = 2\times10^{37}(\frac{10^{17}}{\nu})^{1.175}\left[10^{10}(\frac{\nu}{10^{17}})^{-3.2}t^{-.85} + 10(\frac{\nu}{10^{17}})^{-1.2}t^{.75} + 5\times10^{5}(\frac{\nu}{10^{17}})^{-3.5}t^{1.1} + 0.1(\frac{\nu}{10^{17}})^{0.25}t^{2.1}\right]^{-1}$
10^{10}	$L(t,\nu) = 1.6\times10^{35}(\frac{10^{17}}{\nu})^{1.175}\left[10^{9}(\frac{\nu}{10^{17}})^{-3.2}t^{-0.85} + 0.1(\frac{\nu}{10^{17}})^{1.2}t^{0.75} + 5\times10^{5}(\frac{\nu}{10^{17}})^{-3.5}t^{1.1} + 0.001(\frac{\nu}{10^{17}})^{0.25}t^{2.1}\right]^{-1}$

see some significant amount of radiation emanating from the surface of the medium.

- $\tau_{0.1-10} > 0.7$ ensures that we have some significant absorption happening at the beginning of the simulation (i.e. the emitted radiation is not simply moving unobstructed through the medium).
- $\tau_{0.1-10}(0.1\text{ sec})/\tau_{.1-10}(t_f) > 2$ ensures that there is some change in the optical depth over the course of the simulation. This means that there is some dynamical feedback between the radiation and the medium over the course of the simulation time.

Now that we have defined what we are searching for in our simulations, we can present our findings and determine which combinations of n_0 and H provide an environment where we observe significant absorption that also significantly varies over the course of the simulation.

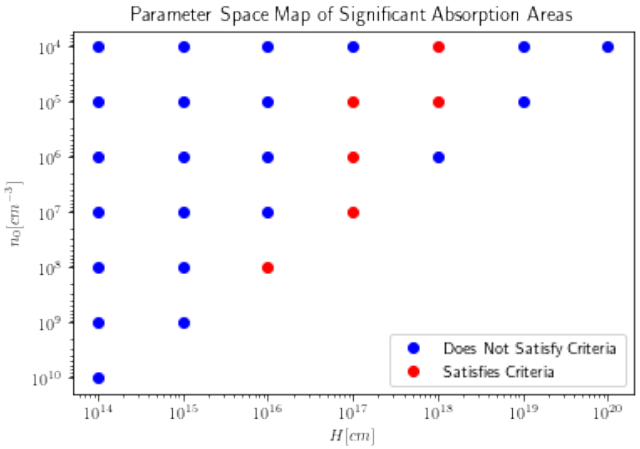

Figure 2. A map showing the parameter space where the criteria is satisfied for "significant and interesting absorption", as defined in section 3.

3.1 Burst Classification

Table 2 and figure 2 summarize our results with respect to which bursts satisfy our criteria for "significant and time-variable absorption". We see that significant and time-variable absorption occurs only for the following combinations of n_0 and H (presented as ordered pairs of the form (n_0 [cm^{-3}], H [cm])): $(10^8, 10^{16})$, $(10^7, 10^{17})$, $(10^6, 10^{17})$, $(10^5, 10^{17})$, $(10^5, 10^{18})$, $(10^4, 10^{18})$. Outside of this range, we can intuitively understand the simulation failing our criteria through one of two mechanisms:

1. The medium is not dense or extended enough, and the optical depth remains very low for the entire duration of the simulation. The radiation is then passing through the medium without ever being significantly absorbed.
2. The medium is very dense and/or very extended, causing the optical depth the be very large throughout the duration of the simulation. Thus, nearly all the radiation is being absorbed and there is no dynamical feedback between the medium and the radiation field.

While a larger and more refined grid search in the (n_0, H) parameter space is needed to make a conclusive statement about where the interesting absorption occurs, we make the following conjecture based on our results: significant and time-variable absorption of GRBs emitted within dense environments occurs when $10^{56}(\frac{H}{1\text{ cm}})^{-3} \leq \frac{n_0}{1\text{ cm}^{-3}} \leq 10^{59}(\frac{H}{1\text{ cm}})^{-3}$.

3.2 Implications for AGN Disks

When mapping conditions on n_0 and H into conditions on location in an AGN disk and SMBH mass, one must pick a particular AGN

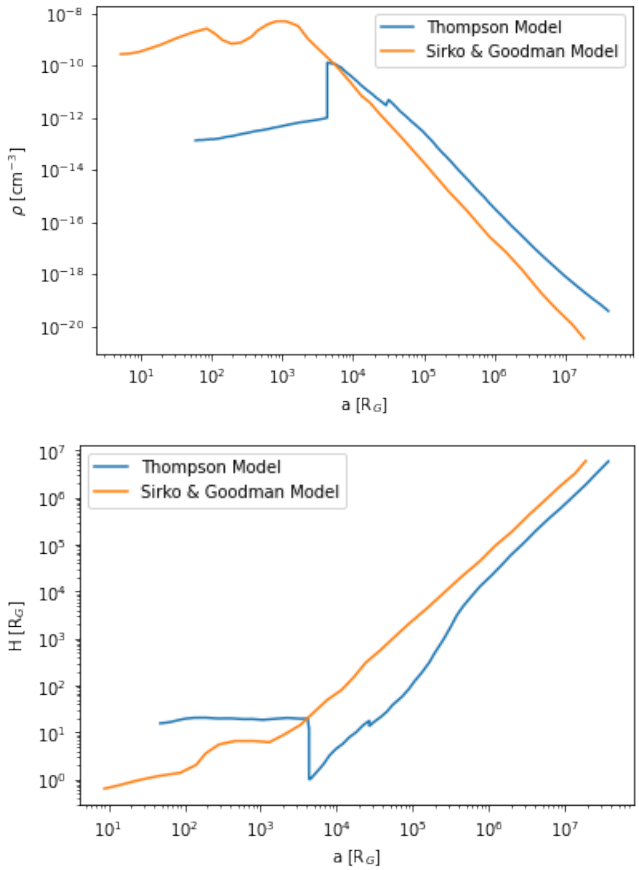

Figure 3. The mass density (top) and scale height (bottom) of the Thompson and Sirko/Goodman AGN disk models as a function of radial position in the disk (in units of gravitational radii). The mass density refers to the density in the plane of the disk, while the scale height encodes information about how quickly the density falls of as we move out of the plane of the disk.

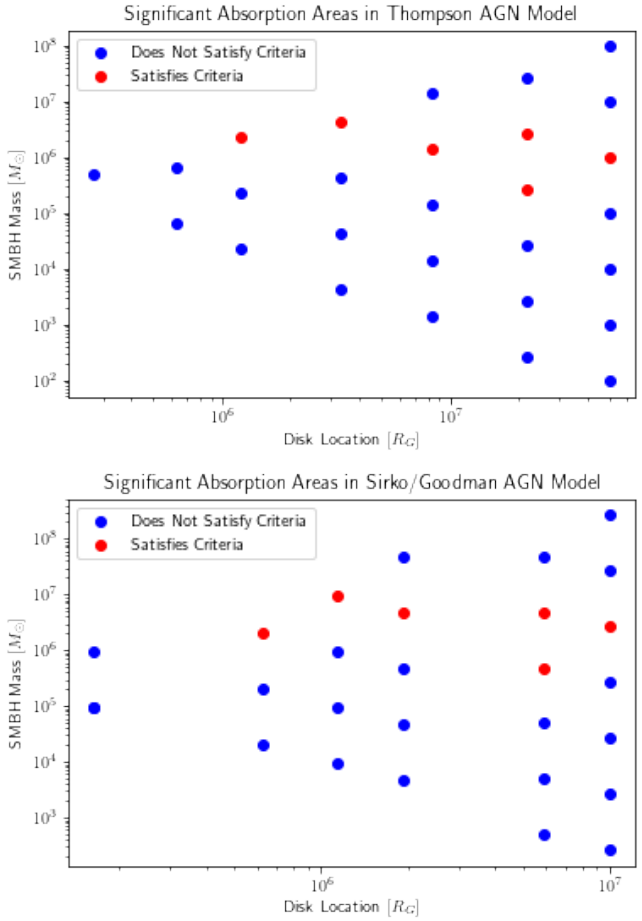

Figure 4. A parameter space mapping of where we see significant and time-variable absorption for both the Thompson (top) and Sirko/Goodman (bottom) AGN models. The red dots indicate simulations where our criteria for significant absorption is met, while the blue dots indicate the opposite. These parameter-space maps are complementary to figure 2 and provide a better intuition for the physical conditions for significant absorption. However, they suffer from the fact that the significant absorption visually follows a more complicated pattern than is shown in figure 2, where we could more easily make a reasonable conjecture for the full parameter space of where significant absorption occurs.

accretion disk model to use. There are multiple reasonable choices here, such as the Shakura-Sunyaev disk model (Shakura & Sunyaev 1973), the Sirko & Goodman model (Sirko & Goodman 2003), or the Thompson model (Thompson et al. 2005). Both the Sirko & Goodman model and the Thompson model are improvements on the Shakura-Sunyaev model in that they are specific to AGN disks (as opposed to a general accretion disk). In particular, the Sirko & Goodman model is thought to be the better model of inner AGN disks, while the Thompson model is thought to be the better model of outer AGN disks (Fabj et al. 2020). We thus map our conditions in (n_0, H) - space into conditions on location and SMBH mass for the Thompson and Sirko/Goodman models separately.

Figure 3 shows the density and scale height profiles for both of the AGN disk models we are considering. The density shown in the figure is the density in the plane of the disk (the central density). In order to map n_0 and H to disk location and SMBH mass, we first convert n_0 to ρ_0 by multiplying n_0 by the mass of a proton. Using the AGN models, we can then find the radial location in the disk that this ρ_0 corresponds to. After finding this, we can use what we know about the scale height in the AGN model to map the scale height to SMBH mass using the relation $R_G = GM/c^2$.

Using the method above, we can easily create figures that are complementary to figure 2, but rather than showing the simulations in the (n_0, H) parameter space, we show the simulations in the (disk location, SMBH mass) parameter space. Figure 4 shows this for both the Thompson and Sirko/Goodman AGN models. Based on these plots, we make the following conjecture that acts in a complementary way to the conjecture made in section 3.1: significant and time-variable absorption of GRBs emitted within dense environments occurs only in when the mass of the SMBH falls within a band between $10^5 M_\odot$ and $10^7 M_\odot$. Again (as with the earlier conjecture) to make a more conclusive statement, we need to perform a larger and more refined grid search. This is left to future work, however.

4 CONCLUSIONS & DISCUSSION

In this work, we presented a grid of simulations investigating the absorption of long gamma-ray bursts emitted from within dense environments. We presented a reasonable definition of what "significant and time-variable" absorption means in this context and then proceeded to present which of our simulations met this definition. Our results led us to make the conjecture that significant and

Table 2. We present the average optical depth in the 0.1 - 10 keV range at 0.1 seconds and at t_f for each of the simulations run. Also shown is the ratio of average optical depth at 0.1 seconds to the average optical depth at t_f. An additional column is added to indicate whether the simulation satisfies all three of our criteria for "significant absorption" to have occurred (the precise definition of this is given in section 3).

(n_0 [cm^{-2}], H [cm])	$\tau_{0.1-10}(t_f)$	$\tau_{0.1-10}(0.1sec)$	$\frac{\tau_{0.1-10}(0.1sec)}{\tau_{0.1-10}(t_f)}$	Criteria Satisfied?
$(10^4, 10^{14})$	10^{-8}	10^{-8}	1	False
$(10^4, 10^{15})$	10^{-8}	10^{-8}	1	False
$(10^4, 10^{16})$	10^{-8}	10^{-8}	1	False
$(10^4, 10^{17})$	10^{-8}	0.00334899425	334893.44	False
$(10^4, 10^{18})$	1.2×10^{-8}	54.03	4423044698.52	True
$(10^4, 10^{19})$	340.8339	624.5311	1.832	False
$(10^4, 10^{20})$	6017.0066	6330.0984	1.05203	False
$(10^5, 10^{14})$	10^{-8}	10^{-8}	1	False
$(10^5, 10^{15})$	10^{-8}	10^{-8}	1	False
$(10^5, 10^{16})$	10^{-8}	10^{-8}	1	False
$(10^5, 10^{17})$	1.2×10^{-8}	21.5751	1766187112.71	True
$(10^5, 10^{18})$	4.7158×10^{-8}	587.747	12463110228.87	True
$(10^5, 10^{19})$	5093.21	6293.80	1.2357	False
$(10^6, 10^{14})$	10^{-8}	10^{-8}	1	False
$(10^6, 10^{15})$	10^{-8}	10^{-8}	1	False
$(10^6, 10^{16})$	1.2×10^{-8}	1.2×10^{-8}	1	False
$(10^6, 10^{17})$	4.715×10^{-8}	425.944	9032104121.61	True
$(10^6, 10^{18})$	1565.67	6116.14	3.9063	False
$(10^7, 10^{14})$	10^{-8}	10^{-8}	1	False
$(10^7, 10^{15})$	1.2×10^{-8}	1.2×10^{-8}	1	False
$(10^7, 10^{16})$	4.7×10^{-8}	4.7×10^{-8}	1	False
$(10^7, 10^{17})$	4.2×10^{-7}	5331.47	12742732795.14	True
$(10^8, 10^{14})$	1.2×10^{-8}	1.2×10^{-8}	1	False
$(10^8, 10^{15})$	4.71×10^{-8}	4.71×10^{-8}	1	False
$(10^8, 10^{16})$	4.18×10^{-7}	1916.41	4580404727.08	True
$(10^9, 10^{14})$	4.7×10^{-8}	4.7×10^{-8}	1	False
$(10^9, 10^{15})$	4.18×10^{-7}	4.18×10^{-7}	1	False
$(10^{10}, 10^{14})$	4.18×10^{-7}	4.18×10^{-7}	1	False

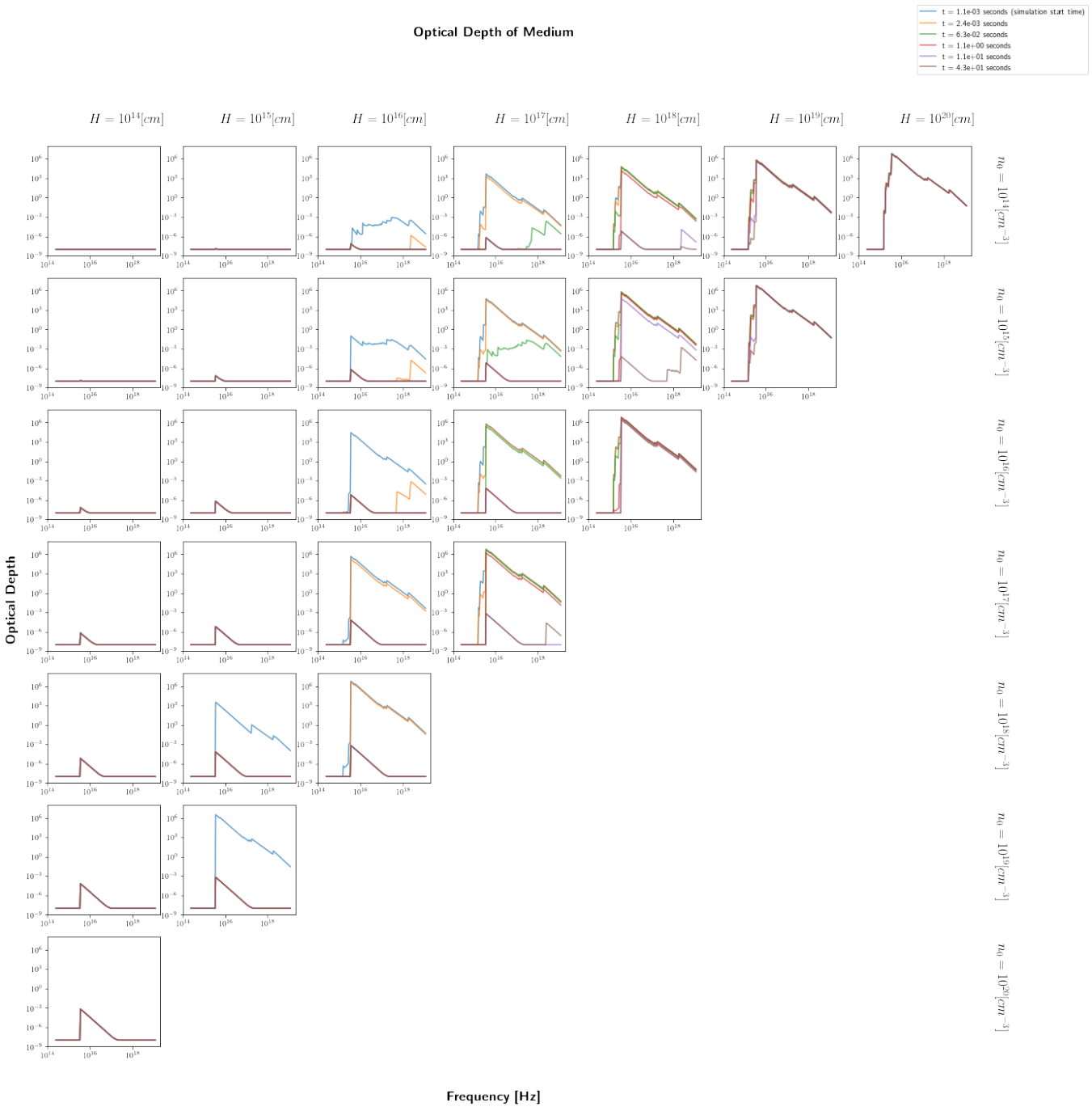

Figure 5. Optical depth as a function of frequency at various times during the simulation. Plots are placed on a grid of the possible values of n_0 and H. The grid is laid out such that H increases to the right in a logarithmic fashion from 10^{14} cm to 10^{20} cm and n_0 increases down the grid from 10^4 cm^{-3} to 10^{10} cm^{-3}. Missing graphs in the grid here represent simulations with column density $Hn_0 \geq 10^{24}$ cm^{-2}, which we omit from our analysis. Each plot shows optical depth at five separate times: ($t = t_{min}$, $t = 0.0024$ sec, $t = 0.063$ sec, $t = 1.1$ sec, $t = 11$ sec, $t = 43$ sec). The times are chosen such that we can see the optical depth during important times in the burst's lifetime. Each of the first three times are time during the prompt emission phase where the ionization of the medium is rapidly changing. The time $t = 1.1$ seconds is a time when the initial ionization of the medium is likely over and the burst is still in its prompt emission phase. $t = 11$ seconds is almost right at the peak of the prompt emission, and $t = 43$ seconds is when the burst is well into its afterglow phase. We see that optical depth (and hence, overall absorption) increases with increasing scale height and increasing number density.

time-variable absorption of LGRBs in dense environments only occurs in a certain band of (n_0, H) parameter space, in particular, only when $10^{56}(\frac{H}{1\text{ cm}})^{-3} \leq \frac{n_0}{1\text{ cm}^{-3}} \leq 10^{59}(\frac{H}{1\text{ cm}})^{-3}$. We then transformed our findings in the (n_0, H) parameter space to findings in the (disk location, SMBH mass) parameter space by choosing two popular AGN models. Here we found that for both AGN models, significant and time-variable absorption seems to only occur in a narrow band of SMBH masses, namely when the mass is between $10^5 M_\odot$ and $10^7 M_\odot$.

While our findings have focused on specific AGN models, the

Figure 6. A grid of plots laid out in the same way as figure 5. Missing graphs in the grid again represent simulations with column density $Hn_0 \geq 10^{24}$ cm^{-2}, which we omit from our analysis. Input bolometric luminosity is represented by blue lines and output bolometric luminosity (i.e. the "post-absorbtion" luminosity emerging from z_{max}) is represented by red lines, both as functions of time. One can clearly observe overall absorption increasing as both n_0 and H increase. This is not surprising given what we see in figure 5 where optical depth (and absorption) also increases with increasing n_0 and H.

simulations themselves only assume that the density of the medium along the line-of-sight falls off as a Gaussian. Thus, our findings in the (n_0, H) parameter space apply to any environment where the density falls off in this manner. As discussed at various points throughout this paper, a larger grid search is needed to fully characterize the parameter space where interesting absorption occurs. The hope, however, is that this provides a starting point for others to work from. Additionally, while this paper focused solely on long GRBs, short GRBs are expected to be found in roughly equal amounts in the environment of AGN accretion disks. We then also hope that the task of investigating the effect of dense media on short GRB spectra will be investigated in the future.

ACKNOWLEDGEMENTS

The author acknowledges support by NSF award AST-2006839.

DATA AVAILABILITY

All the data from this work will be shared upon reasonable request to the authors.

REFERENCES

Achterberg A., Gallant Y. A., Kirk J. G., Guthmann A. W., 2001, Monthly Notices of the Royal Astronomical Society, 328, 393
Band D., et al., 1993, ApJ, 413, 281
Belczynski K., Perna R., Bulik T., Kalogera V., Ivanova N., Lamb D. Q., 2006, ApJ, 648, 1110
Böttcher M., Dermer C. D., Crider A. W., Liang E. P., 1999, A&A, 343, 111
Campana S., Lazzati D., Perna R., Grazia Bernardini M., Nava L., 2021, A&A, 649, A135
Cantiello M., Jermyn A. S., Lin D. N. C., 2021, ApJ, 910, 94
Fabj G., Nasim S. S., Caban F., Ford K. E. S., McKernan B., Bellovary J. M., 2020, MNRAS, 499, 2608
Fong W., Berger E., 2013, The Astrophysical Journal, 776, 18
Gehrels N., Ramirez-Ruiz E., Fox D., 2009, Annual Review of Astronomy and Astrophysics, 47, 567
Golant R., Sironi L., 2022, in American Astronomical Society Meeting Abstracts. p. 109.04
Graham M. J., et al., 2020, Phys. Rev. Lett., 124, 251102
Granot J., Panaitescu A., Kumar P., Woosley S. E., 2002, ApJ, 570, L61
Grishin E., Bobrick A., Hirai R., Mandel I., Perets H. B., 2021, MNRAS, 507, 156
Gröbner, M. Ishibashi, W. Tiwari, S. Haney, M. Jetzer, P. 2020, A&A, 638, A119
Hjorth J., et al., 2003, Nature, 423, 847
Ivezić Ž., MacLeod C., 2014, in Mickaelian A. M., Sanders D. B., eds, Vol. 304, Multiwavelength AGN Surveys and Studies. pp 395–398 (arXiv:1312.3966), doi:10.1017/S1743921314004396
Kasliwal V. P., Vogeley M. S., Richards G. T., 2015, MNRAS, 451, 4328
Kelly B. C., Bechtold J., Siemiginowska A., 2009, ApJ, 698, 895
Kouveliotou C., Meegan C. A., Fishman G. J., Bhat N. P., Briggs M. S., Koshut T. M., Paciesas W. S., Pendleton G. N., 1993, ApJ, 413, L101
Kozłowski S., 2016, The Astrophysical Journal, 826, 118
Krawczynski H., Treister E., 2013, Frontiers of Physics, 8, 609
Lazzati D., Perna R., Ghisellini G., 2001, Monthly Notices of the Royal Astronomical Society, 325
Lazzati D., Perna R., Morsony B. J., Lopez-Camara D., Cantiello M., Ciolfi R., Giacomazzo B., Workman J. C., 2018, Phys. Rev. Lett., 120, 241103
MacLeod C. L., et al., 2010, The Astrophysical Journal, 721, 1014
Mochkovitch R., Hernanz M., Isern J., Martin X., 1993, Nature, 361, 236
Mushotzky R. F., Edelson R., Baumgartner W., Gandhi P., 2011, ApJ, 743, L12
Panaitescu A., Kumar P., 2000, ApJ, 543, 66
Perna R., Lazzati D., 2002, ApJ, 580, 261
Perna R., Lazzati D., Cantiello M., 2021a, ApJ, 906, L7
Perna R., Tagawa H., Haiman Z., Bartos I., 2021b, ApJ, 915, 10
Perna R., Artale M. C., Wang Y.-H., Mapelli M., Lazzati D., Sgalletta C., Santoliquido F., 2022, MNRAS, 512, 2654
Peterson B. M., 2001, in Aretxaga I., Kunth D., Mújica R., eds, Advanced Lectures on the Starburst-AGN. p. 3 (arXiv:astro-ph/0109495), doi:10.1142/9789812811318_0002
Robinson P. B., Perna R., Lazzati D., van Marle A. J., 2009, Monthly Notices of the Royal Astronomical Society, 401, 88
Rossi E., Lazzati D., Salmonson J. D., Ghisellini G., 2002, in Ouyed R., ed., Beaming and Jets in Gamma Ray Bursts. p. 88 (arXiv:astro-ph/0211020)
Sari R., Piran T., Narayan R., 1998, ApJ, 497, L17
Shakura N. I., Sunyaev R. A., 1973, A&A, 24, 337
Sirko E., Goodman J., 2003, Monthly Notices of the Royal Astronomical Society, 341, 501
Spitkovsky A., 2008, ApJ, 682, L5
Stanek K. Z., et al., 2003, ApJ, 591, L17
Thompson T. A., Quataert E., Murray N., 2005, The Astrophysical Journal, 630, 167
Wang Y., Lazzati D., Perna R., 2022,
Yang Y., Bartos I., Fragione G., Haiman Z., Kowalski M., Marka S., Perna R., Tagawa H., 2021, arXiv e-prints, p. arXiv:2105.02342
Yuan C., Murase K., Guetta D., Pe'er A., Bartos I., Mészáros P., 2021, arXiv e-prints, p. arXiv:2112.07653
Zhu J.-P., Zhang B., Yu Y.-W., Gao H., 2021a, ApJ, 906, L11
Zhu J.-P., Wang K., Zhang B., Yang Y.-P., Yu Y.-W., Gao H., 2021b, ApJ, 911, L19
Zu Y., Kochanek C. S., Kozłowski S., Udalski A., 2013, The Astrophysical Journal, 765, 106

This paper has been typeset from a TEX/LATEX file prepared by the author.